

# Numerical Modeling of the Large-Scale Erosion, Sediment Transport, and Deposition Processes of the Genesis Flood

John Baumgardner, Logos Research Associates.

## Abstract

This paper describes a numerical model for investigating the large-scale erosion, transport, and sedimentation processes associated with the Genesis Flood. The model assumes that the dominant means for sediment transport during the Flood was by rapidly flowing turbulent water. Water motion is driven by large-amplitude tsunamis that are generated along subduction zone segments as the subducting plate and overriding plate, in a cyclic manner, lock and then suddenly release and slip rapidly past one another. While the two adjacent plates are locked, the sea bottom is dragged downward by the steadily sinking lithospheric slab beneath. When the plates unlock, the sea bottom rapidly rebounds, generating a large-amplitude tsunami. Theory for open-channel turbulent flow is applied to model the suspension, transport, and deposition of sediment. Cavitation is assumed to be the dominant erosional mechanism responsible for degradation of bedrock as well as for erosion of already deposited sediment. The model treats the water on the surface of the rotating earth in terms of a single vertical layer but with variable bottom height. Illustrative calculations show that with plausible parameter choices average erosion and sedimentation rates on the order of 9 m/day (0.38 m/hr) occur, sufficient within a 150-day interval during the Flood to account for some 70% of the Phanerozoic sediments that blanket the earth's continental surfaces today.

**Note:** This paper is a revision of an ARJ paper published in February 2016. After that paper's publication the author discovered a problem in the numerical formulation that invalidated some of that paper's main conclusions. The numerical problem has been repaired in this present version. Details of the numerical issue involved and how it was repaired are provided in Appendix H.

**Keywords:** global Genesis Flood, catastrophic plate tectonics, giant tsunamis, turbulent sediment transport, cavitation erosion, open channel flow, shallow water approximation

## Introduction

Accounting for the thick sediment sequences that blanket the surfaces of the continents is a paramount issue for understanding the physical aspects of the Genesis Flood. In continental platform regions, such as the heartland of the US, sequences of fossil-bearing sediments are commonly 2000 m or more in thickness (Prothero and Schwab 2004). They also typically display astonishing horizontal continuity (e.g., Ager 1973). Just what sort of physical processes could have moved such huge volumes of sediment and arranged it in such orderly, laterally extensive layers within the span of a single year, as Scripture requires? As a preliminary exercise one can make rough estimates of the erosion, sediment transport, and deposition rates that are needed. If we assume that most of the primary deposition occurred within the interval of 150 days during which “the water prevailed on the earth” (Genesis 7:24), we can compute an average deposition rate over that interval needed to produce a column of sediment, say, 1800 m thick, which is the mean value over the continents today. Dividing 1800 m by 150 days yields a time-averaged rate of deposition of 12 m/day (0.5 m/hr or  $1.4 \times 10^{-4}$  m/s). It also suggests a comparable time-averaged rate of erosion.

The large lateral extent of most of the layers suggests significant transport distances. Let us assume that the average distance between the sites of erosion and deposition is 500 km ( $5 \times 10^5$  m) and that the average speed of the water is 20 m/s (45 mph). A typical sediment particle is therefore in suspension for  $(5 \times 10^5 \text{ m}) / (20 \text{ m/s}) = 2.5 \times 10^4$  s (6.9 hr). If the input and output of the pipeline, so to speak, is the erosion/deposition rate of  $1.4 \times 10^{-4}$  m/s, then the average suspended sediment load distributed vertically through the sheet of flowing water must be  $(1.4 \times 10^{-4} \text{ m/s}) \times (2.5 \times 10^4 \text{ s}) = 3.5 \text{ m}$ . This requires that the depth of the flowing water be great enough and also its turbulence intense enough to sustain this sort of suspended load. From these simple estimates it is obvious that any viable candidate mechanism likely involves coherent sheets of turbulent water at least many tens of meters deep sweeping over the land surface at velocities of at least several tens of m/s. Since these are time-averaged estimates, when the likelihood of significant time variation, even episodicity, is taken into account, the peak water depths and speeds must have been substantially higher.

What might have caused water to move with such vigor across the continent surfaces? The mechanism assumed in this paper is a logical consequence of the large amount of subduction of oceanic lithosphere that occurred during the Genesis Flood (Baumgardner 2003). In today's world, the overriding plate is locked against the adjacent subducting plate along most of the earth's more than 65,000 km of subduction zones. Elastic rebound of the overriding slab typically occurs in sudden jerks, or rupture events. Rupture takes place when the stress reaches a level at which the asperities locking the two plates along the fault surface break, resulting in sudden motion along the fault and release of considerable seismic or earthquake energy. It seems likely that this same locking and sudden rupture process also occurred during the Flood, except much more frequently. For a plate speed of 2 m/s and a subduction angle of 45°, only about an hour is needed to pull down the overriding plate by 5000 m. Sudden rupture of such a locked zone generates an earthquake and resulting tsunami with huge amplitude, larger than any witnessed in recorded history since the Flood. In our illustrative calculations we arbitrarily assume 16 subduction zones, each 1670 km in length, that unlock successively after being locked for 96 minutes to unleash a giant tsunami somewhere in the global ocean every six minutes. The numerical calculations show that such forcing is more than adequate to achieve and maintain the water velocities required. For locked faults that slip and rebound in this manner, peak water velocities reach near 200 m/s and mean water column velocities attain values of many tens of m/s. The turbulence is strong enough to maintain many meters of sediment in suspension as water sweeps across the continental surface. Turbulence is the physical mechanism that allows and maintains such high volume and long-distance transport of sediment.

This paper represents a revision of a paper (2013) I presented at the Seventh International Conference on Creationism. The main difference in the previous paper and this one is the mechanism for driving the water motion. In the previous paper, I invoked tides raised by near encounters of a moon-sized body with the earth. In this paper tsunamis generated by the locking and sudden slip and rebound of fault segments along subduction zones, an expected aspect of catastrophic plate tectonics, are the primary driving mechanism for the turbulent water. The numerical treatments of the water flow, the sediment suspension, the erosion, and the sediment deposition, however, are largely the same as described in the 2013 paper. To save the interested reader of this paper from repeatedly needing to refer to the previous paper to understand the details of the treatments and methods I apply in this paper, I have reproduced those details here as Appendices A–G.

## Mathematical Formulation

The emphasis of this paper is using numerical modeling to explore large-scale erosion, sediment transport, and deposition processes that operated during the Genesis Flood as inferred from the sediments blanketing the continents today. Prominent features of the sediment record, as discussed in the Introduction, suggest that sheets of turbulent water sweeping over the continent surface must have played an important role. Such water motion is in the general category of turbulent boundary layer flow, which is one of great practical interest and one that has been studied experimentally for many years. In the hydrologic engineering community, this type of water flow is referred to as open channel flow. Examples of open channel flows include rivers, tidal currents, irrigation canals, and sheets of water running across the ground surface after a rain. The equations commonly used to model such flows are anchored in experimental measurements and decades of validation in many diverse applications. It is the turbulence of the flowing water in such flows that keeps the sediment particles in suspension. The *Journal of Hydraulic Engineering* is but one of several journals that has published a wealth of papers on turbulent open channel flow and sediment transport over the past many decades.

Appendix A summarizes the observations, experiments, and efforts to formulate a mathematical description of fluid turbulence over the past two centuries. A description of turbulent fluid flow provided almost a century ago by the British scientist L. F. Richardson (1920) is still valid today. His description is a flow whose motions are characterized by a hierarchy of vortices, or eddies, from large to tiny. These eddies, including the large ones, are unstable. The shear that their rotation exerts on the surrounding fluid generates smaller new eddies. The kinetic energy of the large eddies is thereby passed to the smaller eddies that arise from them. These smaller eddies in turn undergo the same process, giving rise to even smaller eddies that inherit the energy of their predecessors, and so on. In this way, the energy is passed down from the large scales of motion to smaller and smaller scales until reaching a length scale sufficiently small that the molecular viscosity of the fluid transforms the kinetic energy of these tiniest eddies into heat.

When a fluid is moving relative to a fixed surface, the speed of the fluid, beginning from zero at the boundary, increases—first rapidly, and then less rapidly—as distance from the surface increases. The region adjacent to the surface in which the average speed of the flow parallel to the surface is still changing, at least modestly, as one moves away from the surface is known as the boundary layer. When

the speed of the fluid over the surface is sufficiently high, the boundary layer becomes turbulent and becomes filled with eddies that can span a large range of spatial scales. Appendix B summarizes some of the important features of turbulent boundary layers, including the discovery that the mean velocity profile within the turbulent boundary layer is very close to a logarithmic function of distance from the boundary. The parameters specifying the profile can be determined simply from the thickness of the layer and the mean flow speed.

The theory of open channel flow applies this mathematical representation of a turbulent boundary layer to describe sediment suspension, transport, and deposition by turbulent water flow for cases where the width of the flow is much greater than the water depth. Appendix C provides the derivation of a mathematical expression, Eq. (A9), for the sediment carrying capacity of a layer of turbulent water as a function of sediment particle size. This expression is utilized in the numerical treatment to quantify the sediment suspension of the water flow. The expression requires the particle settling speed for each of the particle sizes that is assumed in the model. Appendix D describes how these settling speeds may be obtained via empirical fits to experimental data.

### Source of the Sediment

Obviously, an important issue in the formation of the earth's sediment record is the origin of the sediment. From the rock record it is clear that there were pre-Flood continental sediments. However, for sake of simplicity, these sediments are ignored in the illustrative examples we present. Instead, it is assumed that the sediment deposited during the Flood is all derived from erosion of continental bedrock during the Flood itself. In terms of erosional processes, we restrict our scope to the mechanism of cavitation, again for simplicity. We suspect, however, that contributions from other processes by comparison were small. We further assume that the cavitation erosion of crystalline continental bedrock results in a distribution of particle sizes corresponding to 70% fine sand, 20% medium sand, and 10% coarse sand. Here the fine sand fraction also includes the clay and silt, which are assumed to flocculate to form particles that display settling behavior identical to that of fine sand. Mean particle diameters for these three size classes are 0.063 mm, 0.25 mm, and 1 mm, respectively. In this model we neglect carbonates which in the actual rock record represent on the order of 30% of the total sediment volume.

We recognize that it is difficult to imagine how feldspar, even when reduced by cavitation to 0.063 mm particle sizes and smaller, might be

transformed to clay minerals in the brief time span available during the Flood. We acknowledge that a significant portion of the clay in the shales and mudstones in the Phanerozoic sediment record may well have been derived from shales and mudstones of the pre-Flood earth. For example, the Precambrian tilted strata exposed in the inner gorge of the Grand Canyon, rocks that include the Unkar Group, the Nankowep Formation, and the Chuar Group, display total thicknesses of about two miles, mostly of shale and limestone (Austin 1994). Even more impressive, the Mesoproterozoic (Precambrian) Belt Supergroup, exposed in western Montana, Idaho, Wyoming, Washington, and British Columbia, is mostly mudstone (shale, fine sand, and carbonate) and up to 8 mi in thickness (Winston and Link 1993). These examples hint that there may have been a vast quantity of mudrocks on the pre-Flood earth, possibly enough to account for most of the clay and carbonate rocks in the Flood sediment record. Exploring the consequences of initial conditions that include a substantial layer of pre-Flood mudstone sediments is an attractive task for future application of this model.

Appendix E provides a description of the cavitation submodel. It is implemented in the numerical code by means of Eq. (A11). Note that this treatment of cavitation includes a cavitation threshold velocity of 15 m/s below which no cavitation, and hence no erosion, occurs. Appendix E also describes the criteria for deposition and for erosion of already deposited sediment.

Given that the average thickness of Flood sediments on the continents today is about 1800 m, it is not surprising that a numerical model capable of eroding, transporting, and depositing that much sediment will yield sediment thicknesses in some locations that significantly exceed that average value. In early tests it was found that the calculations become unstable unless some degree of isostatic compensation is allowed in locations where the sediment thicknesses become large. Appendix F describes how isostatic compensation is included. Symmetrical compensation is applied for the negative loads that arise from bedrock erosion.

To describe the water flow over the earth in a quantitative way, the numerical model makes use of what is known as the shallow water approximation. This approximation requires that the water depth everywhere be small compared with the horizontal scales of interest. The depth of the ocean basins today—and presumably also during the Flood—is about four kilometers. By contrast, the horizontal grid point spacing of the computation grid for the cases we describe in this paper is about 120 km. The expected water depths over the continental regions, where our main interest lies, are yet much smaller

than those of the ocean basins. Hence the shallow water approximation is entirely appropriate for this problem. That approximation allows the water flow over the surface of the globe to be described in terms of a single layer of water with laterally varying thickness. What otherwise would be an expensive three-dimensional problem now becomes a much more tractable two-dimensional one.

Appendix G outlines the mathematical approach for solving for the water velocity and water height over the surface of the earth as a function of time. The approach involves solving what are known as the shallow water equations on a rotating sphere. These are Eqs. (A12) and (A14) in Appendix G. They express, respectively, the conservation of mass and the conservation of linear momentum. They are solved in a discrete manner using what is known as a semi-Lagrangian approach on a mesh constructed from the regular icosahedron as shown in fig. 1.

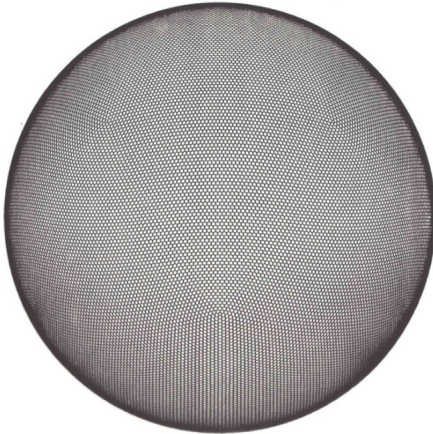


**Fig. 1.** Computational grid used in illustrative cases. Constructed from the regular icosahedron, this grid provides an almost uniform discretization of the spherical surface. It has 40,962 cells with an average cell width of about 120 km for the surface of the earth.

A separate spherical coordinate system is defined at each grid point in the mesh such that the equator of the coordinate system passes through the grid point and the local longitude and latitude axes are aligned with the global east and north directions. The semi-Lagrangian approach, because of its low levels of numerical diffusion, is also used for horizontal sediment transport. Seven layers of fixed thickness are used to resolve the sediment concentration in the vertical direction, with thinner layers at the bottom and thicker layers at the top of the column. These same numerical methods have been applied and validated in one of the world's foremost numerical weather forecast models, a model known as GME developed by the German Weather Service in the late 1990s (Majewski et al. 2002).

Water motion is driven by large-amplitude tsunamis that are generated along subduction zone

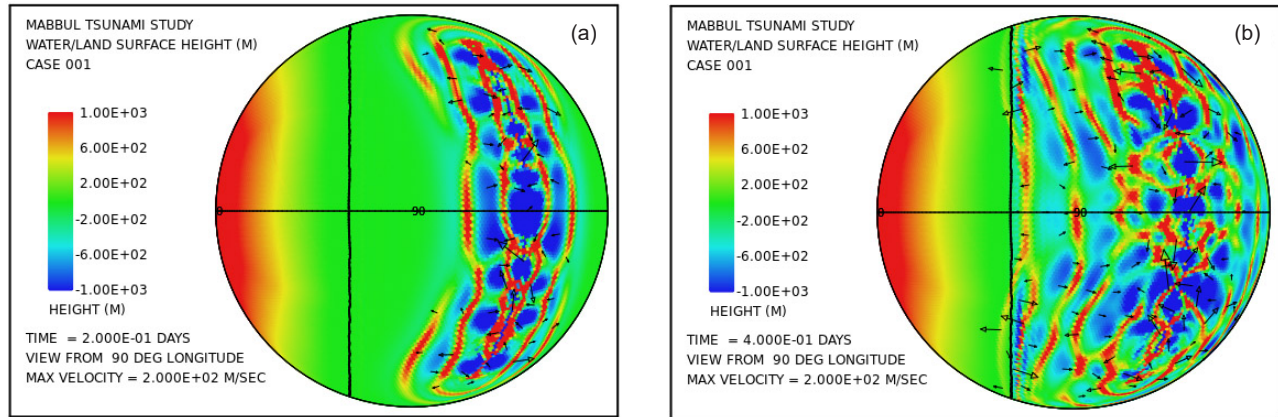
segments as the subducting plate and overriding plate, in a cyclic manner, lock and then suddenly release and rapidly slip past one another. While the adjacent two plates are locked, the sea bottom is dragged downward by the steadily sinking lithospheric slab beneath. When the plates unlock, the sea bottom rapidly rebounds, generating a large-amplitude tsunami. For the cases shown in this paper, zones of subduction are placed along meridians, between latitudes of  $60^{\circ}\text{N}$  and  $60^{\circ}\text{S}$ , at longitudes of  $-126^{\circ}$  and  $126^{\circ}$  in one case and  $-99^{\circ}$  and  $153^{\circ}$  in the other. These longitudes are chosen to exploit symmetries in the grid. The  $120^{\circ}$  interval along each of the two meridians is divided into eight  $15^{\circ}$  segments. Subduction is assumed to be occurring along all of these segments at a rate of about 2 m/s at an angle of  $45^{\circ}$ . While the plates at the subduction zone are locked, the seafloor along each of the segments is assumed to be moving downward at a rate of about  $2 \sin(45^{\circ}) = 1.4 \text{ m/s}$  because of the steady downward motion of the subducting lithospheric slab beneath. Every six minutes, one of the 16 segments is allowed to unlock and slip, allowing the bottom of the trench to rebound to its nominal, undepressed height. The amplitude of the rebound of the trench bottom is about  $1.4 \text{ m/s} \times 16 \times 360 \text{ s} = 8060 \text{ m}$ . This impulsive uplift of the  $15^{\circ}$  segment of trench bottom initiates a tsunami that travels across the 4000 m deep ocean at a speed of about 200 m/s.

Fig. 2 displays a pair of snapshots, at times of 4.8 hours and 9.6 hours from the beginning of the calculation, of the disturbances of the water surface height generated by the successive rebounding of the ocean bottom in the subduction zone located along the meridian at  $126^{\circ}$  longitude. A similar train of tsunami disturbances is generated at the subduction zone located along the meridian at  $-126^{\circ}$  longitude. In this calculation there is continent in the shape of a spherical cap to the left of the vertical black line.

Other distributions of subduction zone were examined, including a single zone along the meridian at  $180^{\circ}$  longitude, and also a single zone along the equator from  $90^{\circ}$  to  $270^{\circ}$  longitude. The other distributions gave qualitatively similar results as those of the illustrative cases presented below.

### An Illustrative Case

To illustrate the global sediment patterns we choose a simple geometry of a single circular continent, centered at the equator and zero degrees longitude, covering 35% of the earth's surface. The ocean bottom surrounding the continent is taken to have a uniform height of  $-4000 \text{ m}$  relative to the mean sea level. The height of the continent at its center is  $1500 \text{ m}$  relative to mean sea level and



**Fig. 2.** Plots of water surface height at (a) 4.8 and (b) 9.6 hours after the beginning of a calculation in which the locking and sudden release of subduction zone fault segments located along the meridian at  $126^\circ$  longitude in the deep ocean generates a train of large-amplitude tsunami waves that begin to invade a circular supercontinent centered at  $0^\circ$  latitude and  $0^\circ$  longitude, located to the left of the heavy vertical line. Water/land surface height is relative to the mean sea level. The initial height of the land surface varies from  $-200$  m at the continent edge to  $1500$  m at its center.

smoothly decreases to  $-200$  m at its edge. Initially the water is at rest with its surface at sea level. The continent surface is assumed everywhere to consist of crystalline bedrock. The earth is assumed to be spinning at its current rate of rotation.

Fig. 3 provides an overview of erosion, transport and sedimentation that unfolds during the initial 50 days in this model. It uses pairs snapshots, at times of 25 and 50 days, showing by means of color, respectively, (i) the water/land surface height above initial sea level, (ii) the instantaneous thickness of sediment suspended by the turbulent flow, (iii) the cumulative bedrock erosion, and (iv) the net cumulative amount of sediment remaining on the surface as a result of the ongoing processes of deposition and erosion. Arrows in plots (a) and (b) represent the velocity of the water column but clipped to a maximum amplitude of  $200$  m/s. Arrows in plots (c)–(h) represent the water velocities at the bottom of the water column just above the land surface. For better clarity, these velocities have been clipped at  $30$  m/s.

Plots (a) and (b) in fig. 3 reveal the presence of tsunamis across much of the deep ocean with amplitudes in many areas exceeding  $1500$  m. These two plots also reveal the presence of a slow, large-scale sloshing, an oscillation of harmonic degrees one and two, as indicated by the distribution of red and blue, whose spatial orientation changes with time. The highly turbulent water flow over the continent is sufficient to suspend many meters of sediment over lower elevation regions of the continent as indicated in plots (c) and (d). Areas with the largest amounts of suspended sediment are those over which a large tsunami is currently passing.

Plots in Fig. 3 (e) and (f) reveal that most of the bedrock erosion occurs along the continent margin.

Since in the cavitation model the erosion rate varies as the sixth power of the difference between the water speed and the cavitation onset speed ( $15$  m/s), it is not surprising for erosion to be most intense at the continental margin where the tsunamis encounter an abrupt decrease in water depth and horizontal water speed changes dramatically. The black contour line along the perimeter of the continent marks the depth of  $300$  m below sea level. Note that the most intense erosion is oceanward of this  $-300$  m contour line. The cumulative volume of bedrock erosion is enough to cover the surface of the entire continent with sediment to a mean depth of  $184$  m after 25 days and  $519$  m after 50 days, reflecting an average erosion (and deposition) rate over 50 days of a bit more than  $10$  m/day. Plots (g) and (h) display the cumulative net result of sediment deposition and sediment erosion. Note that the continent is being progressively buried with sediment, from the coast toward the interior, with the lower elevation coastal zone accumulating the greatest sediment thicknesses. Fig. 4 provides snapshots at times of 100 days and 150 days for the same case and same fields as fig. 3. In plots (a) and (b) note that the sedimentation has buried the original higher topography in the interior of the circular continent. The patterns of erosion and sedimentation are very similar to the comparable snapshots of fig. 3. The cumulative volume of bedrock erosion is enough to cover the surface of the entire continent with sediment to a mean depth of  $1063$  m after 100 days and  $1385$  m after 150 days, reflecting an average erosion (and deposition) rate over 150 days of  $9.2$  m/day.

Noteworthy is the effectiveness of the tsunamis and the associated water dynamics to emplace hundreds of meters of sediment *on top of the continent*, above the mean sea level. If Genesis 7:24 which states, “And the water prevailed upon the earth one hundred and

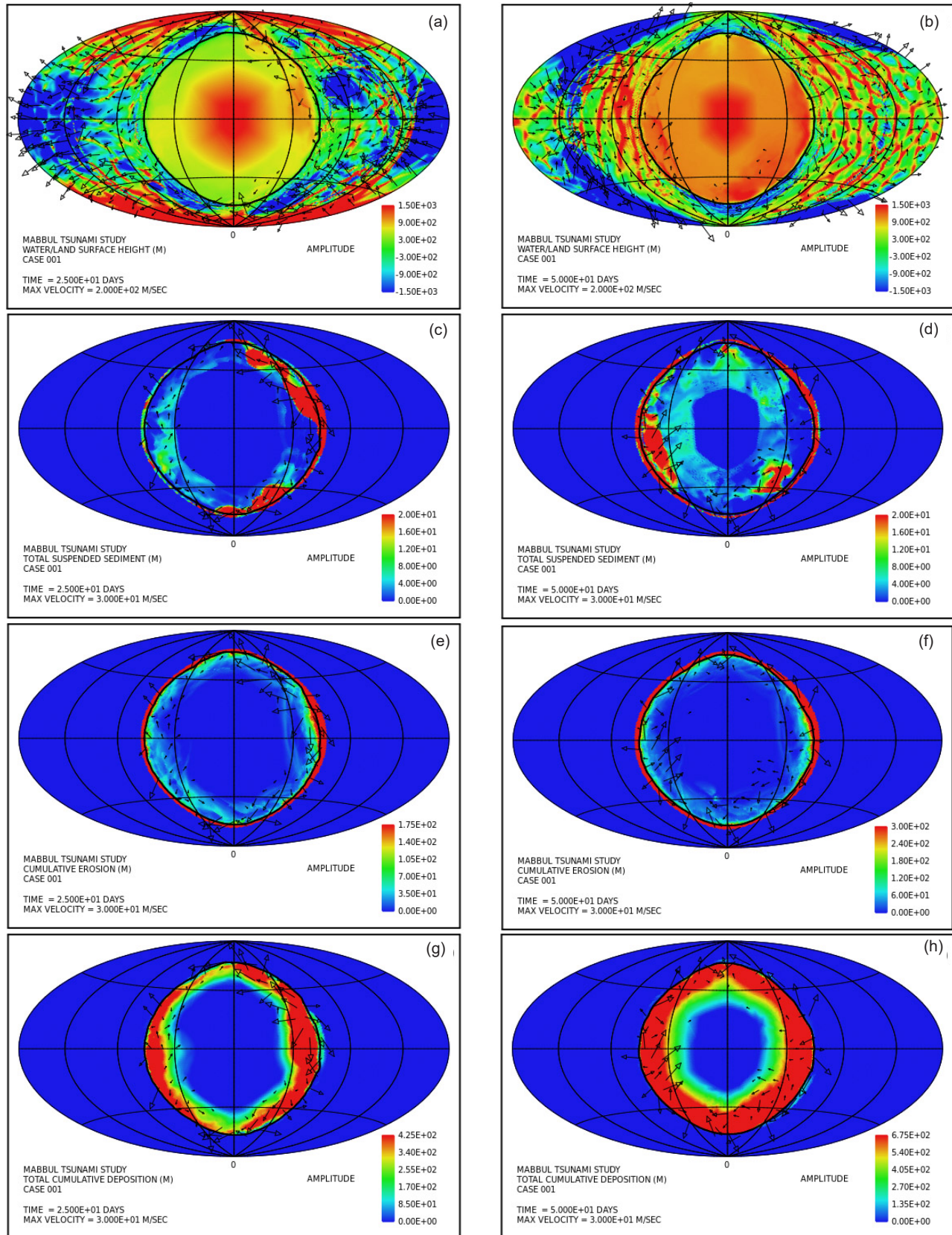


**Fig. 3.** Snapshots at 25 and 50 days of the water/land surface height above sea level (a), (b); the instantaneous thickness of sediment suspended by the turbulent flow (c), (d); the cumulative bedrock erosion (e), (f); and the net amount of sediment on the surface as a result of deposition and erosion (g), (h). Arrows in (a) and (b) represent the mean local velocity of the water column, while in (c)–(h) they represent the water velocity just above the land surface that is used in the erosion submodel.

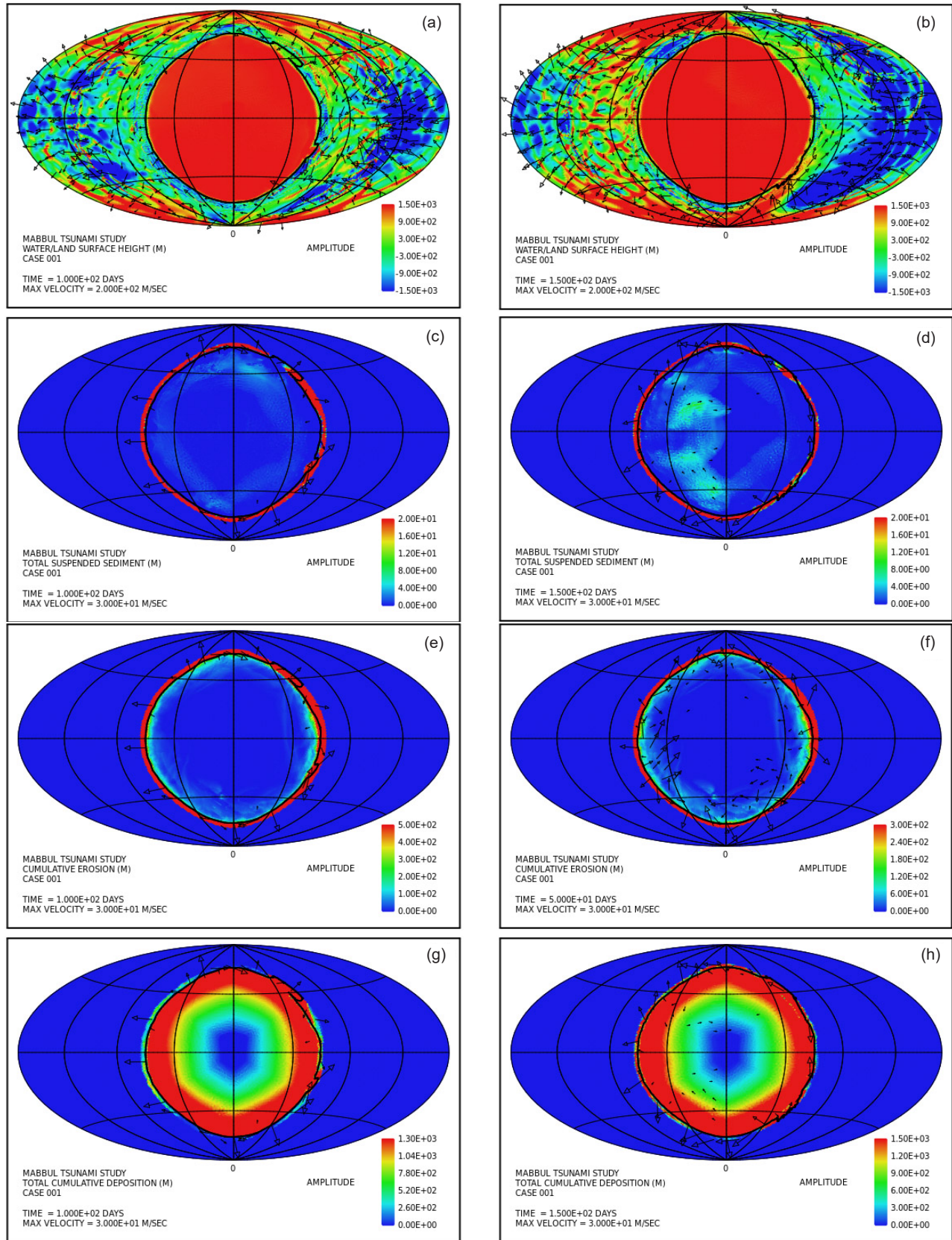


**Fig. 4.** Snapshots at 100 and 150 days of the water/land surface height above sea level (a), (b); the instantaneous thickness of sediment suspended by the turbulent flow (c), (d); the cumulative bedrock erosion (e), (f); and the net amount of sediment on the surface as a result of deposition and erosion (g), (h). Arrows in (a) and (b) represent the mean local velocity of the water column, while in (c)–(h) they represent the water velocity just above the land surface. These snapshots are from the same case as those of fig. 3.

fifty days,” implies that the primary sedimentation of the Flood spanned 150 days, then the almost 1400m of average sediment thickness over this same time interval in the numerical model goes a long way in accounting for the approximately 1800m average thickness of the fossil-bearing sediment record on the continents today.

Fig. 5 provides a more detailed picture of the suspended and deposited sediment when separated into the three assumed sediment classes. As mentioned earlier we assume that the erosional processes, especially cavitation, reduce crystalline bedrock into a mixture of relatively fine particles, 70% with a mean diameter of 0.063mm corresponding

to that of fine sand, 20% with a mean diameter of 0.25mm corresponding to medium sand, and 10% with a mean diameter of 1mm corresponding to coarse sand. Fig. 5 displays the lateral distribution of suspended sediment for each of these size classes at a time of 50 days. It also shows the lateral distribution of the deposited sediment by size class at this same time. The coarse sand has a much higher settling velocity than the fine and medium sand. It is therefore more difficult to maintain in suspension, as fig. 5(e) reveals. It is also the first to fall from suspension as the flow velocity decreases. The coarse sand therefore tends to be deposited closer to its source as indicated in fig. 5(f).

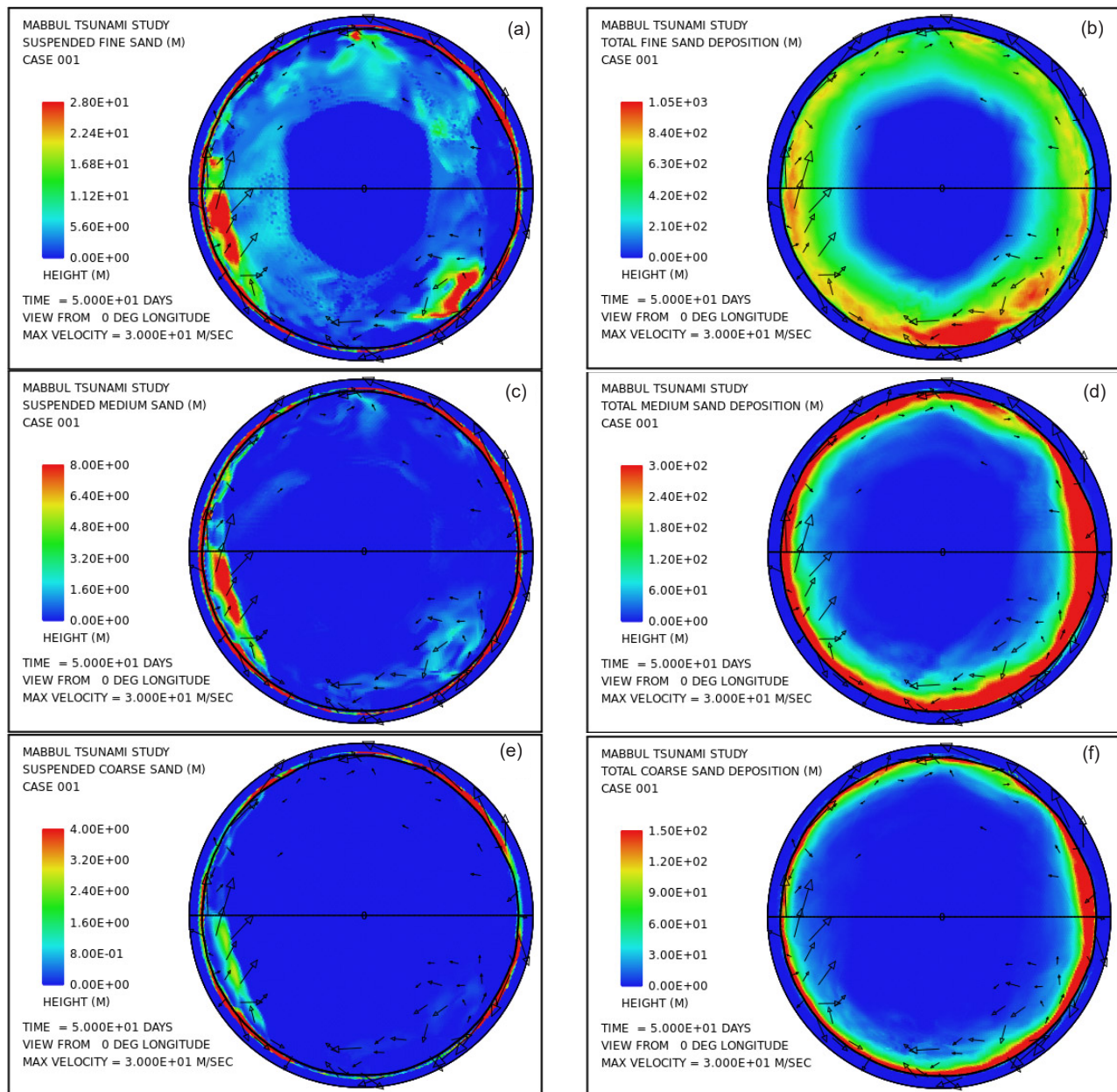


**Fig. 5.** Snapshot at a time of 50 days from the illustrative case: (a) suspended fine sand; (c) suspended medium sand; (e) suspended coarse sand; (b) cumulative deposited fine sand; (d) cumulative deposited medium sand; and (f) cumulative deposited coarse sand. Amplitudes of the plots are scaled to match the 70:20:10 volume ratios produced by bedrock erosion for the three particle size classes.

## A Second Illustrative Case

The case just described used a continent distribution consisting of a single spherical cap, centered at the equator, which covered 35% of the area of the globe. To add a bit more realism a second case is presented, one that preserves the parameter values of the first case but instead of a circular cap uses a Pangean-like continent distribution. Fig. 6 displays snapshots at 50 and 100 days of the water/land surface height relative to nominal (initial) sea level in (a) and (b); instantaneous thickness of sediment suspended by the turbulent flow (c), (d); cumulative bedrock erosion (e), (f); and net cumulative deposition of sediment (g), (h). Arrows denote the mean water column velocity in (a) and (b) and water velocity at the base of the water column in (c)–(h).

This second illustrative case displays the same noteworthy features of the first case including the massive volume of sediment emplaced on the continent surface and erosion concentrated along the continental margins. The cumulative volume of bedrock erosion is enough to cover the surface of the entire continent with sediment to a mean depth of 412 m after 50 days and 835 m after 100 days, reflecting an average rate over the 100 days of 8.4 m/day. This case demonstrates hundreds of meters of sediment emplaced above sea level on top of the continental surface which initially itself was mostly above sea level.

## Discussion

In the context of a reasoned defense of the Genesis Flood there are several major features of the earth's continental surface that cry out for explanation. First is the sheer *volume* of fossil-bearing sedimentary rock present there today. The volume is sufficient to cover the continental surface to an average depth of about 1800 m or about 1.1 mi. What was the source of this massive volume of sediment during the Flood's short time span? Second is the *location* of this huge volume of sediment. It occurs *on top* of the continents, whose surface mostly lies above sea level. This raises the question, what sort of water process might conceivably emplace so much sediment above sea level on top of the land surface? A third issue has to do with the internal *depositional characteristics* of the sediment. Generally speaking, most of the sediment occurs as a vertical succession of horizontal layers, often with vast lateral extent. Such an orderly layer-cake pattern of laterally extensive strata is readily observed, for example, for the sediments exposed in the walls of the Grand Canyon. What sort of transport and depositional process could conceivably generate such uniform layers over such vast horizontal distances?

A fourth prominent feature of the earth's surface includes the so-called *continental shields*, including the Canadian, Baltic, Angaran (Siberian), African, Indian, Australian, and Antarctic shields. These large areas of exposed Precambrian crystalline igneous and high-grade metamorphic rocks have experienced significant erosion (often with more than 1 km of crystalline rock removed), are nearly flat, and have negligible, if any, sediment cover. When in earth history did such intense erosion occur if it was not during the Genesis Flood? And by what sort of process?

This numerical investigation appears to shed at least some new light on each of these important issues. First, in regard to a source for the massive volume of Phanerozoic sediment present in the continental rock record, the numerical study reveals that tsunami-driven cavitation erosion during the time span of the Flood can generate new sediment at a rate sufficient to account for a sizable fraction of the Phanerozoic sediment inventory. The cavitation, occurring at water speeds of several tens of m/s, rapidly reduces crystalline continental crustal rock to sand-sized and smaller particles.

In regard to an explanation for why so much sediment is emplaced on top of the continents when their surfaces mostly lie above sea level, this numerical model also provides especially helpful insight. The calculations show that large-amplitude tsunamis, generated by the rapid plate tectonics of the Flood cataclysm and spaced only minutes apart in time, emplace huge volumes of water onto the continental surfaces and continue doing so as long as the rapid plate motions persist. These tsunamis readily yield a level of turbulence sufficient to suspend the large volumetric rate of sediment produced by cavitation erosion, to transport it to distant locations, and to deposit that sediment in thicknesses reaching hundreds to well over a thousand meters across most of the continental surface. The tsunami-driven flow accounts not only for erosion of significant volumes of sediment but also its emplacement above sea level on top of the continents in coherent patterns with large lateral dimensions.

Aspects of the tsunami-driven water flow are expressed in prominent ways in the internal character of the sedimentary deposits themselves. At a basic level, the water flow associated with a tsunami resembles the ebb and flow of ocean waves on a beach. In a tsunami, there commonly is a surge phase in which high speed, highly turbulent, sediment-laden water invades the land. This generally is followed by a reversal in water direction, reduction in water speed, decline in turbulence, deposition of sediment, and drainage of the water back into the ocean. In this simple picture, the transgressive pulse is erosive and

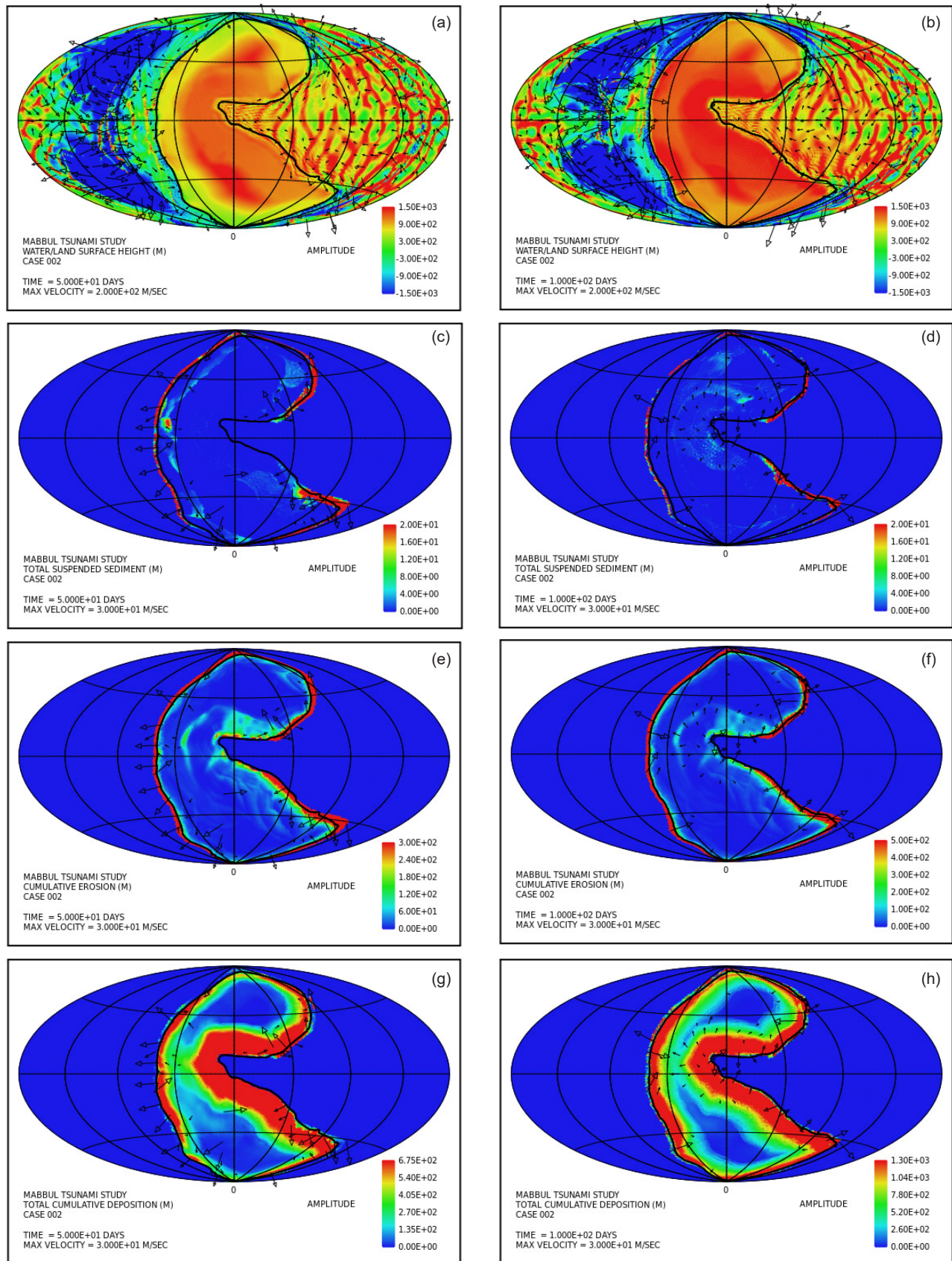


**Fig. 6.** Snapshots at 50 and 100 days from a case with a Pangean-like continent distribution. Colors denote water/land surface height above sea level (a), (b); instantaneous thickness of sediment suspended by the turbulent flow (c), (d); cumulative bedrock erosion (e), (f); and net amount of sediment on the surface as a result of deposition and erosion (g), (h). Arrows denote mean water column velocity in (a) and (b) and water velocity at the base of the water column in (c)-(h).

leads to a beveling of the land surface. By contrast, during the regression phase, as the water is flowing downslope back toward the ocean at much lower speed, the sediment, which the earlier turbulence was able to maintain in suspension, now falls out of suspension and deposits on the recently beveled surface. However, in the setting of the Flood the tsunamis are so frequent that new tsunamis begin invading the land before previous ones have had time entirely to drain back into the ocean. Therefore, individual waves tend to interact and interfere strongly with one another, and the wave pattern becomes very complex. Nevertheless, there is still a pattern of pulses of high-speed turbulent sediment-laden water producing an erosional parting followed by an abrupt drop in water speed and deposition of a layer of sediment. The repeating pattern of sediment layers bounded by erosional partings is so prominent in the sediment record that this author considers this feature to be robust support for the tsunami mechanism. At least at a conceptual level, this mechanism seems sufficiently potent to account for the orderly layer-cake pattern of laterally extensive strata exemplified by the sediments exposed in the walls of the Grand Canyon and elsewhere around the world.

The continental shields represent another major feature of the Phanerozoic rock record that cries out for explanation, especially in the context of the Flood. These shield areas are remarkably flat with little or no erosional channeling and generally display little or no sedimentary deposition subsequent to their intense erosional beveling. An obvious issue is what sort of mechanism is sufficiently potent to erode such hard crystalline rock to depths of up to a kilometer or more within the time span of the Flood and also to do so in such a uniform manner across such laterally extensive areas. The only candidate adequate for such a task this author can imagine are the frequent, large-amplitude tsunamis that arise in the context of catastrophic plate tectonics. Indeed, it is difficult to imagine an alternative mechanism capable of accomplishing such intense and laterally extensive erosion to produce a surface with such astonishing flatness. However, the numerical calculations performed thus far do not show this sort of intense beveling of bedrock within the continental interior. A feature missing in the current model is dynamic surface topography driven by flow of rock inside the earth. This mechanism causes variations of thousands of meters in the height of the continental surface. It is possible that when this physics is included that significant tsunami-driven erosion within the continental interior will be found to arise. A crucial aspect of the model that invites further scrutiny is the locking/slipping mechanics of the

overriding and subducting lithospheric plates responsible in the model for generating the large-amplitude tsunamis. Plate speeds during the Flood, as constrained by the timescale of Genesis chapters 7 and 8 and the widths of new ocean floor generated, must have been at least  $10^8$  times higher than is typical today. On the other hand, as discussed in Appendix F, the strength of mantle rock and possibly also much of the lithosphere was reduced by a similar factor. It is therefore difficult to extrapolate with any degree of confidence today's subduction zone mechanics to the state of affairs that prevailed during the Flood. In today's world, the subducting slab and the overriding plate are always locked, except for brief episodes lasting from seconds to minutes, during which rapid slip occurs, resulting in earthquakes and sometimes large tsunamis. The time between slip events on many subduction zone segments today is measured in terms of centuries. A horizontal speed of 10 cm/yr for one of the plates with the other plate fixed, for example, implies 10 m of slip between plates every 100 years or 20 m of slip every 200 years. How this process might have operated during the Flood when plate speeds were dramatically higher is far from clear. The key issue would seem to be the amount of stress the fault between the plates could sustain without slip occurring. It may well be that the strength reduction due to the runaway process may have affected the lithosphere less than the mantle beneath and allowed relatively higher levels of stress in the locked plates and consequently larger surface deflections between episodes of slip. Further careful study, likely utilizing numerical tools, is urgently needed for this vital issue.

It is to be emphasized that the two illustrative cases presented in this paper are highly simplistic relative to the real earth and the full suite of processes that played a role during the Flood. One of the more glaring deficiencies is that in both cases the continent configuration remained constant, with no continental breakup and no motion of component blocks. Allowing the initial continent configuration to break apart and the resulting blocks to migrate almost certainly will result in major changes in patterns of water flow, erosion, and sedimentation. Neither case included any dynamic topography arising from flow of rock inside the mantle. Such variations in continent surface height can reach several kilometers in amplitude, especially when subduction is occurring near a continental margin.

Furthermore, neither calculation included any changes at all in the location or activity of the subduction zones. Temporal changes in where the tsunamis are generated and their amplitude undoubtedly affect the patterns of water flow, erosion, and sedimentation. Neither of the two cases

included any temporal or spatial changes in the height of the ocean bottom, nor any easily eroded sediment present initially on the continental surface, nor any motions of the deposited sediments due to gravity-driven debris slides, nor any contributions to bedrock erosion from plucking or suspended load abrasion, nor any of a much longer list of processes that undoubtedly affected the sediment distribution in notable ways. In other words, the numerical model described here is merely a beginning, primitive framework for treating the water flow, erosion, and sedimentation of the Flood on a global scale. It is one, however, that has the flexibility to be augmented to address most of the issues just mentioned. Despite its limitations, it is encouraging that the model is able to account for so many of the basic features of the Flood sediment record.

The version of this model presented at the Seventh International Conference on Creationism (Baumgardner 2013) utilized an entirely different mechanism for driving the water motions. In that case the mechanism involved several near approaches with the earth of a moon-sized body that raised large-amplitude tides. That paper suggested that six such near encounters spaced about 30 days apart might plausibly account for the six mega-sequences so prominent in the sediment record and the nearly global erosional unconformities associated with them (Sloss 1963). In view of the results presented in this paper, one might wonder whether these more recent findings supersede or even negate the earlier ones. It is the author's opinion that the two papers and the two forcing mechanisms are mutually compatible. To me it is at least conceivable (but not likely) that both mechanisms might have operated together during the Flood. However, the tsunami mechanism—occurring as a direct consequence of the rapid plate tectonics that logically must have taken place during the Flood—in my view is almost a near certainty. The scenario of a near approach with earth by a moon-sized body described in the 2013 paper was, quite candidly, a near desperation effort on my part to identify an adequate mechanism for driving the water flow. With the tsunami mechanism now yielding such encouraging results, I see little need to pursue the other mechanism any further. The constructive and destructive interference of so many interacting tsunamis leads to occasional pulses with exceptional amplitudes. It is conceivable at least that such infrequent large pulses could account for the megasequence aspects of the record.

## Conclusion

Numerical simulation offers a means for investigating phenomena that are impossible,

either because of their physical scale or the extreme conditions they entail, or both, to explore experimentally in a repeatable manner in the laboratory. The Genesis Flood certainly falls into this category. This paper describes a beginning attempt to apply known physical laws, physical processes that can be investigated in the laboratory, and processes on larger scales that can be studied and characterized by measurements in the present, to model important aspects of this unique cataclysmic event. The numerical model exploits the shallow water approximation to represent water flow in a thin layer on the surface of a rotating sphere corresponding to the earth. It utilizes the theory of open-channel flow to treat the suspension and transport of sediment by turbulent flowing water. As its mechanism for erosion it utilizes cavitation. To drive the water flow it draws upon a currently observable consequence of plate tectonics, namely, the locking and sudden release of the overriding lithospheric plate along its fault contact with the subducting plate in a subduction zone. Today, when the overriding plate unlocks and rebounds, the upward motion of the plate can, and often does, generate a water wave known as a tsunami. During the Flood, when plate speeds were orders of magnitude higher than they are today, the amplitudes of the tsunamis may conceivably have been vastly larger.

In the numerical model such large-amplitude tsunamis drive the global water flow. These tsunamis produce water speeds along the continental margins that immediately exceed the cavitation threshold, leading to intense erosion there of the continental bedrock. The persisting large-scale flow of turbulent water transports the eroded sediment and deposits it in a pattern characterized by large spatial scales. When plate speeds begin to fall due to the exhaustion of gravitational energy driving the motion in the mantle, the tsunamis decrease in frequency and in amplitude, water velocities drop toward zero, and the water that had been pulsing across the continental surface drains back into the ocean basin. In the two illustrative examples, the erosion and deposition rates represent a large fraction of what are needed to account for the 1800 m of sediment on average that blankets today's continental surface.

This numerical model, basic as it is, sheds new light on several important issues relating the Flood. It seems to account (1) for how the continents, which today are mostly above sea level, were inundated during the Flood; (2) for the source of the water responsible for the inundation; and (3) for where that water went at the end of the Flood. It appears to account (4) for how such a huge volume of new sediment could arise during the short time span of the Flood; (5) for how the astonishingly thick

sediment sequences we observe in the sediment record managed to be deposited on top of the normally high-standing continents; and (6) for the vast lateral scales and horizontal continuity of many if not most individual layers within the sediment sequence. Finally, with more realism added in the future it might well also account (7) for the vast regions of flat, deeply beveled Precambrian basement rock known as continental shields.

These promising results invite several future refinements and additions. Examples include augmenting the model to treat continental breakup, motions of the resulting continental blocks, migration of subduction zones, and dynamic topography rising from movement of rock inside the mantle. Such refinements almost certainly will lead to additional insights concerning this cataclysm that in Noah's day so dramatically altered the face of the earth. My prayer is that improved understanding of the processes that generated the fossil-bearing sediment record during the Flood might strengthen the confidence of many in the historical reliability of Genesis 1–11, and hence their confidence in the entirety of Scripture, and thereby strengthen their loyalty and devotion to the Lord Jesus.

## References

- Ager, Derek V. 1973. *The Nature of the Stratigraphical Record*. London, United Kingdom: MacMillan.
- Apsley, David D. 2009. "Structure of a Turbulent Boundary Layer" (Lecture notes from course entitled "Turbulent Boundary Layers," Spring semester, 2009, Manchester University, United Kingdom). <http://personalpages.manchester.ac.uk/staff/david.d.apsley/lectures/turbbl/regions.pdf>.
- Arndt, Roger E.A. 1981. "Cavitation in Fluid Machinery and Hydraulic Structures." *Annual Reviews of Fluid Mechanics* 13 (January): 273–328.
- Austin, Steven A. (ed.) 1994. *Grand Canyon: Monument to Catastrophe*. Santee, California: Institute for Creation Research.
- Bagnold, Ralph A. 1966. "An Approach to the Sediment Transport Problem from General Physics." *Geological Survey Professional Paper 422-I*, Washington, DC: United States Government Printing Office.
- Baker, V.R. 1974. "Erosional Forms and Processes for the Catastrophic Pleistocene Missoula Floods in Eastern Washington." In *Fluvial Geomorphology*, edited by M. Morisawa, 123–148. London, United Kingdom: Allen and Unwin.
- Baumgardner, John. 2013. "Explaining the Continental Fossil-Bearing Sediment Record In Terms of the Genesis Flood: Insights from Numerical Modeling of Erosion, Sediment Transport, and Deposition Processes on a Global Scale." In *Proceedings of the Seventh International Conference on Creationism*, edited by M. Horstemeyer. Pittsburgh, Pennsylvania: Creation Science Fellowship, Inc. [http://media.wix.com/ugd/a704d4\\_70de439475d229ba9231b545de57d670.pdf](http://media.wix.com/ugd/a704d4_70de439475d229ba9231b545de57d670.pdf).
- Baumgardner, John. 2003. "Catastrophic Plate Tectonics: The Physics Behind the Genesis Flood." In *Proceedings of the Fifth International Conference on Creationism*, edited by R. L. Ivey, Jr., 113–126. Pittsburgh, Pennsylvania: Creation Science Fellowship. [http://media.wix.com/ugd/a704d4\\_bfc60d3bb5aad292ce1e8d9384b9eb87.pdf](http://media.wix.com/ugd/a704d4_bfc60d3bb5aad292ce1e8d9384b9eb87.pdf); see also <http://www.logosresearchassociates.org/#!/john-baumgardner/cliy4>.
- Chanson, Hubert. 1997. *Air Bubble Entrainment in Free-Surface Turbulent Shear Flows*. London, United Kingdom: Academic Press.
- Darcy, Henry 1857. *Recherches Expérimentales Relatives au Mouvement de L'eau Dans les Tuyaux. (Experimental Research Relative to the Movement of Water in Pipes)*. Paris, France: Mallet-Bachelier.
- Falvey, Henry T. 1990. *Cavitation in Chutes and Spillways*. Denver, Colorado: US Bureau of Reclamation, Engineering Monograph No. 42.
- Hagen, Gotthilf H.L. 1854. *Über den Einfluss der Temperatur auf die Bewegung des Wassers in Röhren*, 17–98. (*On the Influence of Temperature on the Motion of Water in Pipes*). Mathematische Abhandlungen der Koeniglichen Akademie der Wissenschaften zu Berlin.
- Harris, C.K. 2003. "Suspended Sediment Transport." (Lecture notes from graduate course entitled "Sediment Transport Processes in Coastal Environments" at Virginia Institute of Marine Science). [http://www.vims.edu/~ckharris/MS698\\_03/lecture\\_08.pdf](http://www.vims.edu/~ckharris/MS698_03/lecture_08.pdf).
- Jiménez, José A. Jiménez, and Ole S. Madsen. 2003. "A Simple Formula to Estimate Settling Velocity of Natural Sediments." *Journal of Waterway, Port, Coastal, and Ocean Engineering* 129, no. 2 (March): 70–78.
- Kolmogorov, A.N. 1941a. "The Local Structure of Turbulence in Incompressible Viscous Fluid for Very Large Reynolds Numbers." *Doklady Akademii Nauk SSSR* 30: 299–303. Reprinted in *Proceedings of the Royal Society of London, Series A* 434 (8 July 1991): 9–13.
- Kolmogorov, A.N. 1941b. "Dissipation of Energy in the Locally Isotropic Turbulence." *Doklady Akademii Nauk SSSR* 32:19–21. Reprinted in *Proceedings: Mathematical and Physical Sciences* 434, no. 1890 (8 July 1991): 15–17.
- Majewski, Detlev, Dörte Liermann, Peter Prohl, Bodo Ritter, Michael Buchhold, Thomas Hanisch, Gerhard Paul, Werner Wergen, and John Baumgardner. 2002. "The Operational Global Icosahedral-Hexagonal Gridpoint Model GME: Description and High-Resolution Tests." *Monthly Weather Review* 130 (February): 319–338.
- Momber, A.W. 2003. "Cavitation Damage to Geomaterials in a Flowing System." *Journal of Materials Science* 38, no. 4 (February): 747–757.
- Murai, Hitoshi, Shigeo Nishi, Seiji Shimizu, Yasuyuki Murakami, Yukio Hara, Testushi Kuroda, and Syuichi Yaguchi. 1997. "Velocity Dependence of Cavitation Damage (Sheet-Type Cavitation)." *Transactions of the Japan Society of Mechanical Engineers, Part B* 63, no. 607 (March): 750–756.
- O'Connor, Jim E. 1993. "Hydrology, Hydraulics, and Geomorphology of the Bonneville Flood." *Geological Society of America Special Paper* 274.
- Pope, Stephen B. 2000. *Turbulent Flows*. Cambridge, United Kingdom: Cambridge University Press.

- Prandtl, L. 1905. "Über Flüssigkeitsbewegungen bei Sehr Kleiner Reibung." ("On Fluid Flow with Very Little Friction"). In *Verhandlungen des Dritten Internationalen Mathematiker-Kongresses, Heidelberg*, 484–491. Leipzig: Teubner Verlag.
- Prothero, Donald R., and Fred Schwab. 2004. *Sedimentary Geology: An Introduction to Sedimentary Rocks and Stratigraphy*. 2nd edition, 12–14. New York, New York: W.H. Freeman.
- Reynolds, Osborne. 1883. "An Experimental Investigation of the Circumstances Which Determine Whether the Motion of Water Shall Be Direct or Sinuous, and of the Law of Resistance in Parallel Channels." *Philosophical Transactions of the Royal Society of London* 174: 935–982.
- Richardson, Lewis F. 1920. "The Supply of Energy From and to Atmospheric Eddies." *Proceedings of the Royal Society of London, Series A*, 97, no. 686 (1 July): 354–373.
- Sloss, L. L. 1963. "Sequences in the Cratonic Interior of North America." *Geological Society of America Bulletin* 74 (2) (February): 93–113.
- Staniforth, Andrew. and Jean Côté. 1991. "Semi-Lagrangian Integration Schemes for Atmospheric Models—A Review." *Monthly Weather Review* 119 (September): 2206–2223.
- Stokes, G. 1851. On the effect of the internal friction of fluids on the motion of pendulums. *Transactions of the Cambridge Philosophical Society* 9:8–106.
- Whipple, Kelin X., Gregory S. Hancock, and Robert S. Anderson. 2000. "River Incision into Bedrock: Mechanics and Relative Efficacy of Plucking, Abrasion and Cavitation." *Geological Society of America Bulletin* 112 (3) (March): 490–503.
- Williamson, David L., John B. Drake, James J. Hack, Rüdiger Jakob, and Paul N. Swarztrauber. 1992. "A Standard Test Set For Numerical Approximations to the Shallow Water Equations in Spherical Geometry." *Journal of Computational Physics* 102, no. 1 (September): 211–224.
- Winston, D., and P.K. Link, 1993. "Middle Proterozoic rocks of Montana, Idaho, and Washington: The Belt Supergroup." In *Precambrian of the Conterminous United States*, edited by John C. Reed, Paul K. Simms, R.S. Houston, D.W. Rankin, Paul Karl Link, W. Randall Van Schmus, and P. Bickford, 487–521. Boulder, Colorado: Geological Society of America, *The Geology of North America*, v. C-3.
- Wohl, Ellen E. 1992. "Bedrock Benches and Boulder Bars: Floods in the Burdekin Gorge of Australia." *Geological Society of America Bulletin* 104 (6) (June): 770–778.

## Appendix A: What is Fluid Turbulence?

The importance of the role of turbulence in fluids was clearly recognized in the early part of the 19th century when the pressure drop in water pipes and the drag of water on ships were hydraulics issues of considerable practical concern. It was known that both the pressure drop in pipes and the drag exerted on ships as they moved through the water had two components, one linear and the other approximately quadratic in the fluid velocity. Surprisingly, it was found that only the first one depended on the viscosity of the fluid. In the 1850s G. Hagen and H. Darcy both published careful measurements of fluid flow through large pipes. They both noted that the quadratic component was associated with disordered motion in the fluid and that it became the dominant contribution when the pipes were large and the flow speed became sufficiently high. They speculated that the increased drag was due to the energy spent in creating velocity fluctuations as the flow became turbulent.

G. Stokes (1851) was the first to show that the onset of turbulent flow depends on the ratio of the inertial force of the moving fluid to the viscous forces acting upon it. This ratio is today known as the Reynolds number, named after O. Reynolds, who in the 1870s and 1880s published a series of papers describing results of his careful experimental studies on the transition from laminar to turbulent fluid flow, first in pipes and then in other settings. Reynolds, in an 1883 paper, stressed the importance of this

dimensionless ratio that now bears his name. This ratio, the Reynolds number  $Re$ , is usually expressed as  $Re = uL/\nu$ , where  $u$  is the fluid velocity,  $L$  is a characteristic spatial dimension of the flow, and  $\nu$  is the kinematic viscosity.

In the early 20th century Ludwig Prandtl made an important computational advance by introducing the concept of a fluid boundary layer. In a groundbreaking 1905 paper he showed that the equations for fluid flow could be simplified by dividing the flow field into two regions: a boundary layer in which the fluid viscosity plays a major role and the region outside the boundary layer, where the viscosity can be neglected with no significant effects on the solution. Prandtl's boundary layer theory provided crucial new understanding of skin friction drag and how streamlining reduces drag on airplane wings and other bodies that move relative to a fluid environment.

But what is fluid turbulence? The British scientist L. F. Richardson (1920) described fluid turbulence in poetic fashion as follows:

Big whorls have little whorls  
That feed on their velocity,  
And little whorls have lesser whorls  
And so on to viscosity.

Richardson's picture of turbulence is a flow comprised of a hierarchy of vortices, or eddies, from large to tiny. These eddies, including the large ones, are unstable. The shear that their rotation exerts on

the surrounding fluid generates smaller new eddies. The kinetic energy of the large eddies is thereby passed to the smaller eddies that arise from them. These smaller eddies in turn undergo the same process, giving rise to even smaller eddies that inherit the energy of their predecessors, and so on. In this way, the energy is passed down from the large scales of motion to smaller and smaller scales until reaching a length scale sufficiently small that the molecular viscosity of the fluid transforms the kinetic energy of these tiniest eddies into heat.

In 1941, the Russian A.N. Kolmogorov postulated that for very high Reynolds numbers, the small scale turbulent motions are *statistically isotropic* (i.e., have no preferential spatial direction). In general, the largest scales of a flow are not isotropic, since they are determined by the particular geometrical features of the problem. Kolmogorov's idea was that, in the energy cascade which Richardson described, this geometrical and directional information at the largest scale is lost. This means that the statistics of the smaller scales has a universal character and that they are *the same for all turbulent flows* when the Reynolds number is sufficiently high. He further hypothesized that for very high Reynolds numbers the statistics of small scales are universally and uniquely determined by the viscosity  $\nu$  and the rate of energy dissipation  $\epsilon$ . With only these two parameters, a unique length  $\lambda$  can be obtained by dimensional analysis given by

$\lambda = (\nu^3/\epsilon)^{1/4}$ . This is today known as the Kolmogorov length scale.

Kolmogorov's concept was that turbulent flow is characterized by a hierarchy of scales through which the energy cascade takes place. Dissipation of kinetic energy occurs at scales of the order of Kolmogorov length  $\lambda$ , while the input of energy into the cascade comes from the decay of the large scales, characterized by scale length  $L$ . These two scales at the extremes of the cascade can differ by several orders of magnitude at high Reynolds numbers. In between there is a range of scales (each one with its own characteristic length  $r$ ) that has formed at the expense of the energy of the large ones. These scales are very large compared with the Kolmogorov length, but still very small compared with the large scale of the flow (i.e.,  $\lambda \ll r \ll L$ ). Since eddies in this range are much larger than the dissipative eddies that exist at Kolmogorov scales, hardly any kinetic energy is dissipated in this range. Rather, it is merely transferred to smaller scales until viscous effects begin to become important as the Kolmogorov scale is approached. Within this range inertial effects of the moving fluid parcels are still much larger than viscous effects. Therefore within this inertial range it is possible to neglect the effects of molecular viscosity in the internal dynamics. Although some further details have emerged in the 75 years since Kolmogorov published these ideas, modern understanding of turbulence rests squarely on the basic picture he provided.

---

## Appendix B: Turbulent Boundary Layers

In this paper, the concern is with large-scale erosion and sediment transport and deposition processes over a continental surface driven by a rapidly moving turbulent water layer. This problem is in the general category of open channel flow, which is one of great practical interest and one that has been studied experimentally for many years. Examples of open channel flows include rivers, tidal currents, irrigation canals, and sheets of water running across the ground surface after a rain. The equations commonly used to model such flows are anchored in experimental measurements and decades of validation in many diverse applications. These experiments show that, except for the immediate vicinity of the boundary, the *mean velocity profile* in the turbulent flow regime is very close to being a *logarithmic function of distance from the boundary*. If in addition the boundary is rough due to the presence of, say, discrete sand-sized particles forming the boundary, the mean velocity  $\bar{u}$  (that is, the total velocity with the high frequency fluctuations due to turbulence subtracted away) as

a function of height  $z$  above the boundary is given to good approximation by

$$\bar{u}(z) = 2.5 u_\tau \ln(z/z_o), \quad (\text{A1})$$

where  $u_\tau$  is what is commonly referred to as the shear velocity or friction velocity and  $z_o$  is a number proportional to the size of the roughness elements along the boundary. This result and the brief account of turbulent boundary layer theory that follows are based on lecture notes for a 2009 graduate course entitled "Turbulent Boundary Layers" by David Apsley (2009) at the University of Manchester, UK. Apsley, in turn, relies somewhat on Pope (2000).

The quantity  $u_\tau$ , defined as  $u_\tau = (t_o/\rho)^{1/2}$ , where  $t_o$  is the boundary shear stress and  $\rho$  is the fluid density, should consciously be understood as a measure of the boundary shear stress rather than an actual velocity, even though it has dimensions of velocity and is commonly referred to as such. Using Eq. (A1) the

friction velocity  $u_\tau$  can be computed from the depth  $h$  of the turbulent layer and the mean velocity at  $z=h$  as  $u_\tau = \bar{u}(h)/[2.5 \ln(h/z_o)]$ . Assuming that the boundary roughness arises from fairly well-sorted mineral sediment particles with the usual natural range of particle shape and roundness, the quantity  $z_o$  is given by  $D/30$ , where  $D$  is the characteristic particle size. For purposes of this paper,  $D$  is chosen to be 0.5 mm, the value commonly used to distinguish coarse sand from medium sand. The factor 2.5 is the reciprocal of the von Karman parameter, an experimentally determined quantity, named after Theodore von Kármán, a Hungarian-American aeronautical engineer considered by many to be the preeminent theoretical aerodynamicist of the 20th century.

Eq. (A1) provides a realistic, experimentally validated description of the mean horizontal velocity and the associated turbulence from just a few millimeters above the boundary to the top of the flowing layer. Note that the kinematic viscosity  $\nu$  does not appear. This is because at the surface the drag on the surface is dominated by the roughness of the sediment particles and the turbulence this generates, rather than shearing of the water itself. The representation of the turbulent flow in terms of Eq. (A1) enables one to connect the global water velocity field obtained by solving the shallow water equations on a rotating sphere (the earth) with the more localized model of erosion, sediment transport, and sediment deposition described below.

## Appendix C: Sediment Transport in a Turbulent Boundary Layer

The following treatment of suspended sediment follows closely that provided by Harris (2003) in her lecture notes for a graduate course on sediment transport processes. Suspension of sediment particles occurs when the turbulent velocity fluctuation  $w'$  in the vertical direction is at least as large as the settling speed  $w$  of the particles. Experiments show that the vertical velocity fluctuation  $w'$  due to turbulence is approximately equal to the friction velocity  $u_\tau$ , that is,  $w' \approx u_\tau$  near the bottom of the turbulent layer. A quantity known as the Rouse parameter  $P$ , involving the ratio of  $w$  to  $u_\tau$  and defined as  $P = w/ku_\tau = 2.5w/u_\tau$ , is commonly used as a criterion for suspension. ( $\kappa$  is the von Karman parameter, whose value is 0.4.) Based on experimental observation it is found that for  $P > 2.5$  there is no suspension, for  $1 < P < 2.5$  there is incipient suspension, and for  $P < 1$  there is full suspension. Note that the particle settling speed  $w$ , and hence also the Rouse parameter  $P$ , depends on particle size.

To characterize the sediment load of the turbulent layer of water, it is useful to use the local volume fraction  $c$  of sediment in the flow. If the flow is reasonably uniform in the horizontal direction on spatial scales on the order of the layer thickness, which we shall assume, and is reasonably steady on time scales on the order of our numerical time step, then from mass conservation it can be shown that

$$\partial/\partial z [c w + \langle c' w' \rangle] = 0, \quad (\text{A2})$$

where prime (') denotes the fluctuating component and  $\langle \rangle$  denotes time average. The term  $\langle c' w' \rangle$  represents vertical diffusion of suspended sediment by turbulent eddies. This term can be rewritten in

terms of an eddy diffusivity  $K_s$  as  $\langle c' w' \rangle = K_s \partial c / \partial z$ , and Eq. (A2) can then be rewritten as

$$\partial/\partial z [-w c - K_s \partial c / \partial z] = 0. \quad (\text{A3})$$

Integrating this equation with respect to  $z$  yields

$$-w c = K_s \partial c / \partial z. \quad (\text{A4})$$

This states that for steady, uniform conditions the downward settling of sediment ( $-w c$ ) balances the upward diffusion of sediment by turbulent eddies. Integrating once more with respect to height using  $y$  as the variable of integration yields

$$\ln[c(z)/c(a)] = -w, \quad (\text{A5})$$

where  $a$  is a reference height near the bed where the concentration  $c(a)$  can be specified. In turbulent flow near the bed the eddy viscosity  $K_m$  for momentum is given by  $K_m = \kappa u_\tau z$ , where  $\kappa$  is the von Karman parameter,  $u_\tau$  is the friction velocity, and  $z$  is height. Since the same eddies that diffuse momentum vertically also diffuse mass, one can represent the eddy diffusivity  $K_s$  as  $K_s = \alpha \kappa u_\tau z$ , where  $\alpha$  is a constant of proportionality. For low sediment concentrations  $\alpha \approx 1$ , and for high concentrations a value of 1.35 is commonly used. Substituting this expression for  $K_s$  into the right hand side of Eq. (A5) we find

$$-w = -[w/(\alpha \kappa u_\tau)] \ln(z/a). \quad (\text{A6})$$

Combining Eqs. (A5) and (A6) and using the fact that the Rouse parameter  $P = w/ku_\tau$ , we obtain the following expression for the volume fraction  $c$  of sediment as a function of height  $z$  above the bed

$$c(z)/c(a) = (z/a)^{-P/a}. \quad (\text{A7})$$

This result is valid only near the base of the turbulent layer. To obtain a description that is applicable throughout the turbulent layer, it is necessary to use an eddy diffusivity that decreases more strongly with height. One such functional form commonly used yields an eddy diffusivity profile that is parabolic, decreasing to zero at the top of the turbulent layer at  $z=h$  and approaching  $aku_\tau z$  near the base of the layer. It is expressed as  $K_s = aku_\tau z(1-z/h)$ . Substitution of this quadratic eddy diffusivity into Eq. (A7) yields what is known as the Rouse profile,

$$c_i(z) = c_i(a) \{ [z(h-a)]/[a(h-z)] \}^{-P/a}. \quad (\text{A8})$$

Since the Rouse parameter depends on particle settling velocity which in turn depends on particle size, we divide the sediment into a finite number of sediment classes according to particle size which we designate by the subscript  $i$ . Eq. (A8) then provides a separate vertical distribution of volume fraction for each sediment class.

Integrating Eq. (A8) with respect to height from  $a$  to  $h$ , noting that  $\{ [z(h-a)]/[a(h-z)] \}^{-P/a} = [(h/z-1)]/[(h/a-1)]^{P/a}$ , we obtain the following expression for the carrying capacity  $F_i$  of the flow for each sediment class

$$F_i = [c_i(a)/(h/a-1)^{P_i/a}] \int_a^h (h/z-1)^{P_i/a} dz. \quad (\text{A9})$$

We choose the reference height  $a$  to be constant with a value of 1 cm. Since  $c_i(a)$ , the sediment volume fraction at height  $a$ , is dimensionless, we note that  $F_i$  has units of distance.  $F_i$  represents the total thickness of sediment of class  $i$  that the flow can suspend. For purposes of the computation, because, as explained below, we impose a severe limit on the sediment volume fraction at each height, we take  $c_i(a)$  to be unity. Note that  $F_i$  then depends only on the Rouse parameter  $P_i$  of the sediment class and the depth of the turbulent layer  $h$ . For practical reasons, we divide the height coordinate  $z$  into a number of discrete zones or layers, indexed by  $k$ , and compute a sediment carrying capacity  $F_i^k$  for each layer. The total column carrying capacity  $F_i$  is then given by  $F_i = \sum F_i^k$ , where the summation is over  $k$ . In the illustrative cases we describe later, we use a total of seven vertical layers of fixed thickness to represent the sediment profile in the turbulent flow.

Turbulent water can maintain only a limited volume fraction of sediment in suspension. Based on the work of Bagnold (1966), the limiting volume fraction at any given height in the flow, over all sediment classes, is about 0.09. We impose this limit in each of the vertical layers at each lateral grid point in the computational mesh.

---

## Appendix D: Settling Speed of Sediment Particles

As we have seen, the ability of a turbulent flow to suspend sediment particles and maintain them in suspension depends on the settling velocity  $w$  of the particles. The Rouse parameter  $P$  that occurs as the exponent in the vertical sediment distribution formula (A8) involves the ratio of the settling velocity  $w$  to the friction velocity  $u_\tau$  of the turbulent flow. A great deal of experimental effort has been invested to characterize the settling velocity of sediment particles over the past 60 years. To obtain appropriate values for  $w$  we utilize a simple formula developed by Jiménez and Madsen (2003) that provides a good fit to the experimental measurements for grain sizes between 0.063 mm and 1 mm, covering the range from very fine to coarse sand. This formula is

$$w(d) = Y/(A + B/S), \quad (\text{A10})$$

with  $Y = [(s-1)gd]^{1/2}$  and  $S = 0.25dY/\nu$ , where  $d$  is the nominal grain diameter,  $s$  is the specific gravity of the sediment grains,  $g$  is gravitational acceleration,  $\nu$  is the kinematic viscosity of water, and  $A$  and  $B$  are constants arising from the fit to the data. We assume a specific gravity  $s$  for sand of 2.65, the value for  $g$  to be 9.8 m/s<sup>2</sup>, and a kinematic viscosity  $\nu$  for water of 10<sup>-6</sup> m<sup>2</sup>/s. The values for the constants  $A$  and  $B$  provided by Jiménez and Madsen (2003) are  $A = 0.954$  and  $B = 5.12$ . For each sediment class  $i$  with mean nominal grain diameter  $d_i$  we apply (A10) to obtain the settling velocity  $w_i$  for that sediment class. For the case described in this paper we choose three sediment classes with nominal grain diameters  $d_i$  of 0.063 mm, 0.25 mm, and 1 mm, corresponding to fine sand, medium sand, and coarse sand, respectively. Clay and silt is assumed to flocculate to form particles that display settling behavior identical to that of fine sand.

---

## Appendix E: Erosion and Deposition

At present the erosion model is very simple. Since our interest is capturing the most salient aspects of the global Flood cataclysm in which water velocities reach several tens of meters per second, we neglect erosion processes at low water velocities and instead focus on cavitation-driven erosion which occurs at higher water velocities and results in extreme erosion rates. Cavitation involves the formation of water vapor and air bubbles which occurs when local fluid pressure drops below the vapor pressure of dissolved air (Arndt 1981). Cavitation damage arises when these bubbles are carried into regions of higher pressure and implode in the vicinity of the water-rock interface. The pressure spikes generated by the implosion and collapse of these bubbles are typically on the order of several hundred MPa, or several thousand atmospheres (Momber 2003). Such pressure pulses exceed the shear strength of most silicate minerals. They therefore damage and erode the lattices of individual crystals that comprise a polycrystalline rock (Momber 2003).

Whipple, Hancock, and Anderson (2000) provide the following simple expression to describe the rate  $\dot{e}_c$  of surface degradation in m/s from cavitation erosion

$$\dot{e}_c = E(u - u_{cav})^q, \quad (\text{A11})$$

where  $E$  is a proportionality constant,  $u$  is the flow velocity just above the bed (assumed at height  $z=a$ ), and  $u_{cav}$  is a cavitation threshold velocity. We adopt this simple relationship to represent cavitation in our model.

What values for  $q$ ,  $u_{cav}$ , and  $E$  might be appropriate for representing the extreme conditions expected for a cataclysm on the scale of the Genesis Flood? Experimentally determined values for the exponent  $q$  as large as 7 have been reported (Murai et al. 1997). Falvey (1990) assumes a value for  $q$  of 6. Several authors put  $q$  in the range of 5–7. We choose a value for  $q$  of 6. Note that with  $q$  equal to 6, doubling the difference between  $u$  and  $u_{cav}$  increases the cavitation erosion rate by a factor of 64. The cavitation threshold velocity  $u_{cav}$  depends on the flow depth, fine sediment concentration, dissolved air content, and Reynolds number. Chanson (1997) observes that on chute spillways and bottom outlets, cavitation damage can begin to occur at clear water velocities of between 12 to 15 m/s. Falvey (1990) suggests that cavitation can begin to occur in spillways at velocities as low as 10 m/s. In our cavitation treatment we choose a value for  $u_{cav}$  of 15 m/s.

The multiplicative factor  $E$  in Eq. (A11) is not that well constrained by experimental data. Falvey (1990, 34) mentions an experiment in which a 13 mm hole was produced in concrete over a period of 3 hours by a 30 m/s jet, but almost no details of the experiment are provided. These numbers suggest a cavitation erosion rate of  $1.2 \times 10^{-6}$  m/s. More recently Momber (2003) reports experimental work to measure relative rates of cavitation erosion for various types of rocks and concrete using a cavitation chamber. Crucial details of the experiment are not included in the paper. Nevertheless, erosion rates provided in mg/s and the area of damage from the photographs in the paper imply erosion rates for granite and rhyolite on the order of  $4 \times 10^{-5}$  m/s. In light of the measurements presently available, we view the value we have chosen ( $1 \times 10^{-6}$  m/s for a water speed of 20 m/s) as reasonable. The discovery that cavitation can be usefully applied to rock drilling is prompting laboratory studies pertaining to these applications (e.g., Momber 2003). This suggests that more experimental data for the cavitation regime of extremely high water velocities may soon be forthcoming.

It has also been proposed that cavitation may operate in conjunction with abrasion by suspended sediment particles to give erosion rates much greater than by either process alone. In attempting to account for many field examples of streambed erosion of massive, coarsely jointed rocks, especially features of fluting and pot-holing, Whipple, Hancock, and Anderson (2000), in the context of abrasion erosion by the suspended sediment load, remark:

Although one might argue that much of the suspended sediment flux passes through the system without much interaction with the channel boundaries, channel reaches where joint block plucking is inhibited typically develop significant and stable topographic irregularities, which generate intense vortices that bring the suspended load into contact with the bed. These vortices in fact focus abrasion damage on specific areas of the bed, resulting in the initial development of flutes and potholes. Once flutes and potholes begin to form, a strong positive feedback develops because the developing microtopography of the erosional form enhances and stabilizes the vortex structure, further strengthening the localized attack of abrasion by suspended particles. Finally, it is plausible that the inception of cavitation bubbles down the cores of vortices contributes to the focusing of erosion in flutes and potholes, as has been argued by some previous investigators (Baker 1974; Wohl 1992; O'Connor 1993). If cavitation indeed occurs in

natural systems, the likely onset of cavitation within vortices during high-velocity flow may help explain the apparent dominance of fluting and potholing over abrasion wear by large, vigorously saltating particles. (Whipple, Hancock, and Anderson 2000, 8)

By the phrase, “vigorously saltating particles,” they are referring to bouncing bedload particles as opposed to particles suspended in the turbulent flow. They have already argued that the erosion rate from suspended sediment abrasion, apart from cavitation enhancement, ought to scale with the fifth power of the velocity just above the bed (p. 6, Eq. 10), and hence that it can possibly be comparable to the erosion rate they give for cavitation erosion. The two processes acting together must certainly involve rates much higher than either acting alone. Nevertheless, in our model we include only cavitation erosion and choose a value for  $u_{cav}$  of 15 m/s, a value for  $q$  of 6, and a value for  $E$  of  $0.000001/(20-15)^6=6.4\times 10^{-11}$ , which implies an erosion rate of  $10^{-6}$  m/s or 1 micrometer/s for a flow velocity at of 20 m/s at height  $z = a$ . We believe this to be very conservative for the velocity range in which cavitation occurs.

The deposition treatment is straightforward. Suspended sediment in the bottommost layer which is in excess of the carrying capacity of that layer is declared to be deposition. At each grid point the newly deposited sediment is added, by class, to a sediment deposition array and is also removed from the sediment suspension array for the bottommost vertical layer. This test is performed in the time stepping process after the new time level water column heights and velocities have been computed, after the suspended sediment profiles have been updated to account for the water transport, and after the new sediment carrying capacities have been computed. If the turbulent flow has not reached its capacity to suspend sediment and if the flow is sufficiently rapid to erode the base, we allow for erosion and suspension of the resulting eroded particles.

For our application, we account for the possible presence of a high concentration of sediment in the proximity of the surface. We do this by scaling  $E$  by the factor  $(1-10C)$ , where  $C = \sum_i c_i(a)$  is the sum over all sediment classes of their volume fractions within the height interval 0.01–1 m (layer 1), with this sum restricted by the sedimentation treatment to be no larger than 0.1. This restriction implies that when the total sediment volume fraction within the bottommost layer reaches 0.1, erosion ceases. In addition, we limit  $E$  such that it does not exceed 20%

of the residual column carrying capacity, that is, 0.2 times the difference between the column carrying capacity and the total sediment load. For simplicity, we use these parameter values regardless of the flow depth and Reynolds number. When the bed material is sediment and not crystalline bedrock, we use the same parameters except that we increase  $E$  by a factor of three to account for the relative softness of the sediment. A test is made to ensure that all the existing sediment cover is eroded before any bedrock erosion occurs.

We assume further that cavitation degrades crystalline granitic bedrock into a distribution of particle sizes corresponding to 70% fine sand, 20% medium sand, and 10% coarse sand. This choice is motivated primarily by our assessment of the distribution that is characteristic of the earth’s sediment record. Implicit in this assumed distribution of particle sizes is the additional assumption that clay and silt-sized particles flocculate and behave as fine sand in their settling behavior. In addition, for purposes of this exploratory study, we ignore the carbonate sediments. We also note that experiments that provide a reliable particle size distribution from cavitation acting on crystalline silicate rocks are mostly lacking at this point in time.

After the erosion calculation has been performed, the newly eroded sediment is added to the suspended sediment profile by dividing the eroded sediment thickness, for each sediment class, by the height of the water column and multiplying by layer thickness for the contribution to each layer. Since it is possible in a given layer for the sediment concentration to exceed the carrying capacity, we address this situation. After the new time level water column heights and velocities have been computed, after the suspended sediment profiles have been updated to account for the water transport, and after the new sediment carrying capacities have been computed, but before the erosion calculation has been performed, we allow settling of sediment into the layer below. The amount transferred equals the time step (in seconds) multiplied by the settling rate (in meters per second) of the particular sediment class but limited by the excess of sediment in the layer (in meters) relative to the layer carrying capacity (in meters). We begin the procedure with the topmost layer.

The cumulative amounts of erosion and deposition, as well as the instantaneous amounts of suspended sediment by class, as a function of position over the surface, are tracked as the time stepping proceeds.

## Appendix F: Effect of Sediment Load on Topography

It was found early in the testing the model that sediment thicknesses of several hundreds of meters routinely arise. When such large thicknesses were allowed to augment the original continent topography with no isostatic compensation whatsoever, a type of numerical instability was observed. This behavior involved the formation of localized mounds of sediment, typically a few hundred kilometers across and hundreds of meters high. This topography, in turn, forced the water flow to become concentrated in channels between these sediment mounds and for enhanced deposition to occur on top of the mounds where the flow depths and velocities were small. The higher the mounds grew, the stronger this tendency became. A simple remedy for this problem was to include some degree of isostatic compensation to allow the basement to subside in response to the sediment load above it. The compensation scheme chosen provides no compensation for loads less than 500m, increasing to 10% compensation for a load of 1000m, 20% compensation for a load of 1500m, and 25% compensation for a load of 2000m. For the portion of load in excess of 2000m, 50% compensation is applied. Symmetrical compensation is implemented for the negative loads produced by material removed by bedrock erosion. Certainly, this prescription is only one of many that could have been chosen. Its main features include that the compensation is instantaneous and that the fraction of compensation

increases monotonically with increasing sediment load height. The assumption that the compensation is instantaneous would, at first, seem difficult to justify, even as an approximation. However, when one takes into account the extreme reduction in rock strength throughout the mantle caused by the stress weakening mechanism associated with runaway lithospheric slabs and mantle plumes, it becomes more plausible. Calculations show that the weakening, which starts in the vicinity of a slab or plume that is entering the runaway regime, quickly spreads to encompass the entire mantle. The reduction in rock strength throughout the mantle then approaches a factor of a billion. This reduction in rock strength also affects the lithosphere. It implies a rapid response of the continental lithosphere to surface loading during the Flood while the mantle is in its weakened state.

Such nearly instantaneous compensation was found to suppress the unexpected behavior in an effective manner. However, the behavior may well not be computational but rather may actually be reflecting physical reality. As such, it clearly merits further study. This is especially so given that the tendency of the flow to form mounds of sediment yields more vigorous localized water flow, more intense erosion, and ultimately greater volumes of sediment. However, such further exploration will be deferred until later and is considered beyond the scope of this present paper.

---

## Appendix G: Solving for the Water Flow Using the Shallow Water Approximation

To describe the water flow over the earth we utilize the so-called shallow water equations applied to a rotating sphere. By shallow water it is understood that the water depth is everywhere small compared to the horizontal scales of interest. The ocean basins today have mean depths of about four kilometers while the computation grid for the earth's surface for the cases we describe in this paper has a horizontal grid point spacing of about 120km. The expected water depths over the continental regions where our main interest lies are yet much smaller than those in the ocean basins. The shallow water approximation is therefore an appropriate one for this problem, one that allows the water flow over the surface of the globe to be treated in terms of a single layer of water with laterally varying thickness. What

otherwise would be an expensive three-dimensional problem now becomes a much more tractable two-dimensional one.

The shallow water equations on a rotating sphere may be expressed (Williamson et al. 1992, 213)

$$dh/dt = -h \nabla \cdot \mathbf{u} \quad (\text{A12})$$

and

$$d\mathbf{u}/dt = -f \mathbf{k} \times \mathbf{u} - g \nabla h^t, \quad (\text{A13})$$

where  $h$  is water depth,  $\mathbf{u}$  is horizontal velocity (on the sphere),  $f$  is the Coriolis parameter (equal to  $2\Omega \sin \theta$  for rotation rate  $\Omega$  and latitude  $\theta$ ),  $\mathbf{k}$  is the outward radial unit vector,  $g$  is gravitational

acceleration, and  $h^t$  is the height of the free surface above some spherical reference surface. Here it is assumed that the water is homogeneous in composition, incompressible, and inviscid. If  $h_t$  denotes topography on the sphere, then  $h^t = h + h_t$ . The  $d/dt$  operator is the material or substantial or co-moving time rate of change of an individual parcel of fluid. The  $\nabla$  operator is the spherical horizontal gradient operator and the  $\nabla \cdot$  operator is the spherical horizontal divergence operator. Symbols in bold font correspond to vector quantities. Eq. (A12) is an expression of the conservation of mass, while Eq. (A13) is an expression of the conservation of linear momentum. As mentioned above, this two-dimensional formulation in terms of a single layer in the radial direction is appropriate when the water depth is small in comparison to the important horizontal length scales.

In our problem the water depths above the continental regions are much smaller compared to those in the oceanic regions, and in these continental regions where the water is shallow we expect strong turbulence. Therefore, the assumption that the flow is inviscid is not an appropriate one, and we need to account for the strong drag that occurs at the continent-water interface. A simple means for doing this is to add a bottom friction term on the right hand side of Eq. (A13) of the form  $-\beta \mathbf{u}/(h+1)$ , where  $\beta$  is a scaling parameter with units of m/s. Because the terms in Eq. (A13) have dimensions of force per unit mass, this drag term requires the division by water depth  $h$  to be consistent. The addition of 1 to  $h$  in the denominator is to prevent the overall term from becoming excessively large as the water depth approaches zero. It is also common in ocean models to include in the momentum equation a so-called eddy viscosity term that seeks to represent the effects of turbulence on scales not resolved by the computational grid. The simplest such formulation is a term proportional to the 2-D Laplacian operator  $\nabla^2 = \nabla \cdot \nabla$  on the sphere applied to the velocity field, that is, a term of the form  $\gamma \nabla^2 \mathbf{u}$ , where  $\gamma$  is a scaling parameter with units  $m^2/s$ . Note that  $\gamma$  depends on

the grid resolution. Typical values are  $1 \times 10^{-3}$  for  $\beta$  and  $2 \times 10^{-11}$  for  $\gamma$  when the grid spacing is 120km. Adding these two terms to the right hand side of the momentum Eq. (A13) yields

$$d\mathbf{u}/dt = -f \mathbf{k} \times \mathbf{u} - g \nabla h^t - \beta \mathbf{u}/(h+1) + \gamma \nabla^2 \mathbf{u}. \quad (\text{A14})$$

Note that in continental regions the water depth can decrease to zero. We therefore constrain the water depth  $h$  always to be non-negative and the water velocity  $\mathbf{u}$  to be zero when  $h$  is zero. We also constrain the right hand side of Eq. (A14) to be zero when  $h$  is zero.

Eqs. (A12) and (A14) are solved in discrete fashion on a mesh constructed from the regular icosahedron as shown in fig. 1. A separate spherical coordinate system is defined at each node such that the equator of the system passes through the node and the local longitude and latitude axes are aligned with the global east and north directions. This approach has the advantage that the coordinates are almost Cartesian and only two (tangential) velocity components are needed. A semi-Lagrangian formulation (Staniforth and Côté 1991) of Eqs. (A12) and (A14) is used which involves computing the trajectories during the time step that end at each node. Values for  $h$  and  $\mathbf{u}$  at the beginning of the time step at the starting point of each trajectory are found by interpolating from the known nodal values at the beginning of the time step. Changes in  $h$  and  $\mathbf{u}$  along the trajectory are computed using Eqs. (A12) and (A14). This Lagrangian-like method eliminates most of the numerical diffusional noise that is associated with Eulerian schemes. A second-order accurate interpolation scheme is used to find the starting point values of the trajectories. This formulation using the icosahedral mesh has been carefully validated using the suite of test problems developed by Williamson et al. (1992). It also forms the basis for the global weather forecast model known as GME developed in the late 1990s by the German Weather Service which is now used by more than 20 other nations (Majewski et al. 2002).

## Appendix H: Rationale for the Revision

In early 2018, I discovered a significant problem in the numerical formulation I had been using to model the tsunamis and their dynamics. The problem pertained to the semi-Lagrangian method I applied to transport water across the spherical surface and the approach I had used to guarantee global mass conservation. This transport scheme, although it offers a huge benefit in providing a low level of numerical diffusion (that is, a small amount of smearing out of

fine details), it has the downside that it is not perfectly mass-conserving. Twenty-five years ago when I first implemented the method for problems in which the entire spherical surface was covered with a more or less uniform layer of fluid (e.g., air or water), I utilized a simple strategy to ensure mass conservation. On each time step I merely added or subtracted a tiny uniform correction everywhere to the fluid depth to guarantee that fluid mass was conserved.

Fast-forwarding to 2018, I recognized that the simple scheme I had been using previously to ensure mass conservation was not appropriate for problems which included sudden violent upward displacements of the seafloor and the launching of giant tsunamis. The difficulty I discovered was that there were large errors arising locally where uplifts of the seafloor by several kilometers occurred in a single time step. Moreover, these large errors were not random in sign, which would have allowed them to tend to cancel one another, but instead were consistently negative, meaning that a global positive depth correction on the order of a meter was needed every time step to conserve water mass. Such a correction was being made over the continental areas as well as over deep ocean. It became immediately clear to me that these consistently positive corrections were the explanation for the unexpected continental flooding I had reported in the original 2016 paper and also for a consistently downslope water flow I observed in the model when I included more realistic continental topography.

I found that this problem could be eliminated through two relatively small changes in the formulation. The first change involved correcting most of the large errors associated with the tsunamis locally within the cells in which they occurred. This reduced the total volume of water loss to a small fraction of what it had been before. The second change was to apply no depth correction at all over continental regions and instead to apply all the needed correction, which was now much more modest, exclusively in regions of deep ocean where the water depths were large and the fractional changes were tiny. This strategy stably conserved water volume

and eliminated the tendency for anomalous flooding of the continents.

The present version of this paper highlights results from the same two supercontinent configurations described in the original 2016 paper but with the corrections to the numerical formulation included to eliminate the anomalous continental flooding. The current version also includes a more realistic continental topography, a more conservative cavitation erosion rate, and a smaller amount of isostatic compensation for thick sediment loads and large erosion depths. Each of these three adjustments toward improved realism affect the basic solutions in only minor ways.

Importantly, the current version corrects the prominent incorrect conclusions in the original paper that the frequent, large amplitude tsunamis during the Flood spontaneously caused massive, persisting, and almost complete flooding of the continental surface, in many places by more than a kilometer of water for as long as the tsunamis continued, and that the water motions over the continents were dominated by large anti-cyclonic gyres at high latitudes. The current version reveals instead that the frequent, large amplitude tsunamis deliver pulses of water which reach far into the continental interior and that the overall water motion is similar to the ebb and flow of waves on a beach. The calculations suggest that the amplitude and turbulence of the tsunami pulses enabled them to suspend and transport sediment sufficient to cover the continental surface to an average depth of more than a kilometer during the time frame of the Flood.

John Baumgardner  
June 14, 2018